Direct control of hepatic glucose production by interleukin-13 in mice

Kristopher J. Stanya,[1] David Jacobi,[1,2] Sihao Liu,[1] Prerna Bhargava,[1] Lingling Dai,[1,3] Matthew R. Gangl,[1] Karen Inouye,[1] Jillian L. Barlow,[4] Yewei Ji,[5] Joseph P. Mizgerd,[6] Ling Qi,[5] Hang Shi,[7] Andrew N.J. McKenzie,[4] and Chih-Hao Lee[1]

[1]Department of Genetics and Complex Diseases, Division of Biological Sciences, Harvard School of Public Health, Boston, Massachusetts, USA. [2]CHRU de Tours, Service de Médecine Interne-Nutrition, INSERM U1069, Université François Rabelais, Tours, France. [3]Pharmacogenetics Research Institute, Institute of Clinical Pharmacology, Central South University, Changsha, Hunan, People's Republic of China. [4]MRC Laboratory of Molecular Biology, Cambridge, United Kingdom. [5]Division of Nutritional Science, Cornell University, Ithaca, New York, USA. [6]Pulmonary Center, Boston University School of Medicine, Boston, Massachusetts, USA. [7]Department of Internal Medicine, Wake Forest Health Sciences, Winston-Salem, North Carolina, USA.

Hyperglycemia is a result of impaired insulin action on glucose production and disposal, and a major target of antidiabetic therapies. The study of insulin-independent regulatory mechanisms of glucose metabolism may identify new strategies to lower blood sugar levels. Here we demonstrate an unexpected metabolic function for IL-13 in the control of hepatic glucose production. IL-13 is a Th2 cytokine known to mediate macrophage alternative activation. Genetic ablation of *Il-13* in mice (*Il-13*$^{-/-}$) resulted in hyperglycemia, which progressed to hepatic insulin resistance and systemic metabolic dysfunction. In *Il-13*$^{-/-}$ mice, upregulation of enzymes involved in hepatic gluconeogenesis was a primary event leading to dysregulated glucose metabolism. IL-13 inhibited transcription of gluconeogenic genes by acting directly on hepatocytes through Stat3, a noncanonical downstream effector. Consequently, the ability of IL-13 to suppress glucose production was abolished in liver cells lacking *Stat3* or IL-13 receptor α1 (*Il-13rα1*), which suggests that the IL-13Rα1/Stat3 axis directs IL-13 signaling toward metabolic responses. These findings extend the implication of a Th1/Th2 paradigm in metabolic homeostasis beyond inflammation to direct control of glucose metabolism and suggest that the IL-13/Stat3 pathway may serve as a therapeutic target for glycemic control in insulin resistance and type 2 diabetes.

Introduction

Loss of postprandial glycemic control followed by fasting hyperglycemia is a hallmark of type 2 diabetes (1, 2). The resulting glucotoxicity contributes to metabolic complications, such as pancreatic β cell death and vascular dysfunction (3). Therefore, identification of therapeutic approaches to improve glycemic management will be beneficial for diabetes and related metabolic diseases.

Glucose homeostasis is achieved through tight regulation of its production and utilization. In healthy individuals, these 2 processes are balanced to maintain blood glucose within a narrow physiological range. The liver is the main tissue for glucose production, and the regulation of hepatic gluconeogenic genes, including pyruvate carboxylase (*Pcx*), phosphoenolpyruvate carboxykinase (*Pepck*), fructose-1,6-bisphosphatase (*Fbp1*), and glucose-6-phosphatase (*G6p*) has been extensively studied. During fasting, gluconeogenic genes are induced in the liver by several transcription factors, including forkhead box protein O1 (FOXO1), PPARγ coactivator–1α (PPARGC1α), and cAMP response element–binding protein (CREB) and its coactivators, CREB-binding protein/p300 (CBP/p300) and cAMP-regulated transcriptional coactivators (CRTCs) (4, 5). Conversely, in states of abundant glucose, such as after a meal, insulin suppresses hepatic glucose production through AKT kinases that trigger nuclear exclusion of FOXO1 and CRTC2 in a phosphorylation-dependent manner, thereby relieving transcriptional activities of FOXO1 and CREB (4–6). Transcriptional repression of gluconeogenesis is less understood, although STAT3 has been implicated in this process (7, 8). Interestingly, it has been shown that downregulation of hepatic gluconeogenic genes by feeding is maintained in mice lacking *Akt1/2* and *FoxO1* in the liver (9), indicative of the existence of additional, uncharacterized mechanisms controlling gluconeogenesis (6).

In addition to normal physiological regulation, recent evidence suggests that glucose homeostasis is also modulated by chronic inflammation associated with metabolic stress (10, 11). Genetic models in mice have demonstrated that deletion of key inflammatory mediators improves glucose tolerance in obesity-induced insulin resistance (12). The detrimental effects of proinflammatory pathways, most notably those triggered by Th1 cytokines (e.g., IFN-γ, TNF-α, and IL-1β), on glucose homeostasis are achieved partly through inhibitory serine phosphorylation of IRS1 by JNK. In turn, uncontrolled hyperglycemia could further contribute to chronic inflammation. For example, the activity of NF-κB is increased through O-GlcNAc modification under high-glucose conditions (13). NF-κB is a primary transcription factor downstream of Th1 cytokines, and its activation in the liver promotes systemic insulin resistance (14, 15). Consequently, increased activities of Th2 cytokines (e.g., IL-4 and IL-13) skew the immune response to a Th2 phenotype (16) and restore glucose homeostasis (17–21). Th2 cytokines activate several downstream effectors, including STAT6, PPARγ, and PPARδ, to induce macrophage alternative activation, which dampens inflammation. The Th1/Th2 (or M1/M2) paradigm is thought to play a major role in the progression of white adipose tissue (WAT) inflammation and dysfunction in obesity (22, 23). However, it is unclear whether Th2 cytokines directly interact with metabolic pathways to modulate systemic glucose and lipid homeostasis.

Authorship note: Sihao Liu and Prerna Bhargava contributed equally to this work.
Conflict of interest: The authors have declared that no conflict of interest exists.
Citation for this article: *J Clin Invest.* 2013;123(1):261–271. doi:10.1172/JCI64941.

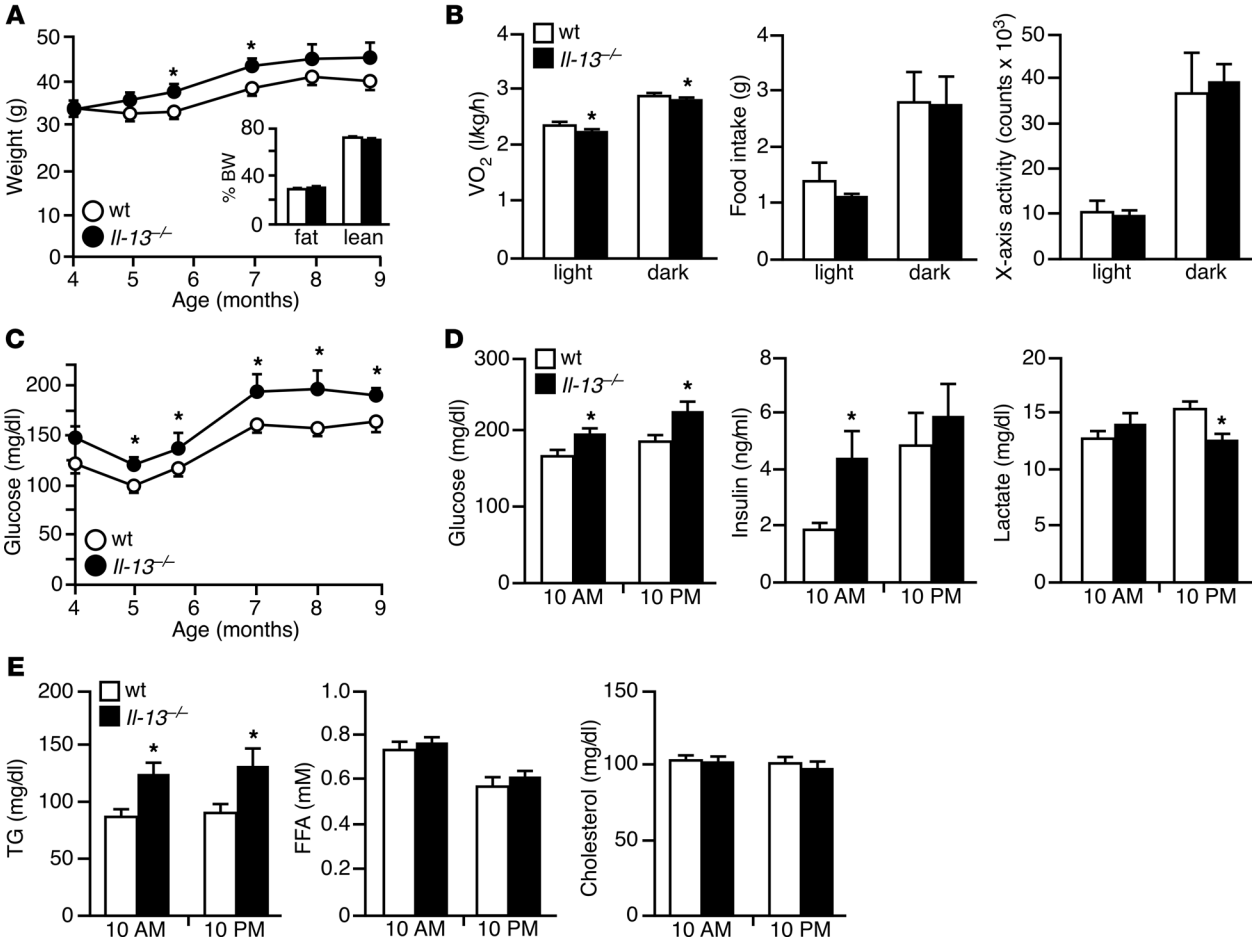

Figure 1

Il-13$^{-/-}$ mice show increased body weight and blood glucose levels. (**A**) Body weight in normal chow–fed WT and *Il-13*$^{-/-}$ mice (C57BL/6 background; n = 7–10 per genotype). Inset: body composition at 7 months of age, determined by DEXA. (**B**) Reduced O_2 consumption, but normal food intake and activity, as determined by metabolic cages in 4-month-old *Il-13*$^{-/-}$ mice. Average values from the light and dark cycles are shown. (**C**) Increased fasting glucose concentrations in *Il-13*$^{-/-}$ mice. (**D**) *Il-13*$^{-/-}$ mice exhibited dysregulated glucose metabolism. Blood glucose, serum insulin, and serum lactate levels of 7-month-old chow-fed WT and *Il-13*$^{-/-}$ mice were measured at 10 AM (fasted state) or 10 PM (fed state). (**E**) TG, FFA, and cholesterol levels of WT and *Il-13*$^{-/-}$ mice were determined at 10 AM and 10 PM. Data are mean ± SEM. **P* < 0.05 vs. WT.

We previously reported that appreciable amounts of IL-13, but not IL-4, were detected in the liver and WAT (17). Several sources of tissue Th2 cytokines have since been identified, including CD4$^+$ T lymphocytes, eosinophils, type I NKT cells (i.e., αGalCer loaded and CDd reactive), nonimmune cells, and a new class of innate lymphoid-2 cells (ILC2 cells; including nuocytes, Ih2 cells, and natural helper cells) and multipotent progenitor type 2 (MPP^{type2}) cells (17, 21, 24–29). In the current study, we sought to determine the role of IL-13 in metabolic regulation. Our data revealed a previously unrecognized IL-13/STAT3 pathway in the control of hepatic glucose metabolism.

Results

C57BL/6 Il-13$^{-/-}$ *mice show glucose intolerance and insulin resistance on normal chow diet.* IL-13 binds to the IL-13 receptor α1 (IL-13Rα1) subunit of the type II receptor complex consisting of an IL-13Rα1/IL-4Rα dimer (30). Both IL-13Rα1 and IL-4Rα were found to be expressed in nonimmune cells, such as hepatocytes (Supplemental Figure 1A; supplemental material available online with this article; doi:10.1172/JCI64941DS1), indicative of potential metabolic functions for IL-13. In light of this observation, we used male *Il-13*$^{-/-}$ mice on the C57BL/6 background as a genetic model to examine the effect of IL-13 depletion on metabolic homeostasis. On normal chow diet (9% fat), C57BL/6 *Il-13*$^{-/-}$ mice progressively gained more weight over a 9-month period than did WT animals (Figure 1A), although fat mass (determined by dual-energy X-ray absorptiometry; DEXA) was not significantly different. Metabolic cage analyses performed on 4-month-old mice, prior to body weight divergence, revealed that C57BL/6 *Il-13*$^{-/-}$ mice had reduced oxygen consumption during both day (light cycle; fasting state) and night (dark cycle; feeding state), with no difference in food intake and physical activity compared with control mice (Figure 1B). Interestingly, *Il-13* gene deletion led to increased fasting glucose levels (6-hour fast) that were detected at 4 months and peaked at 7 months of age (Figure 1C). Blood chemistries at the latter time point were further analyzed at 10 AM and 10 PM without disturbance of sleep/wake cycles (corresponding

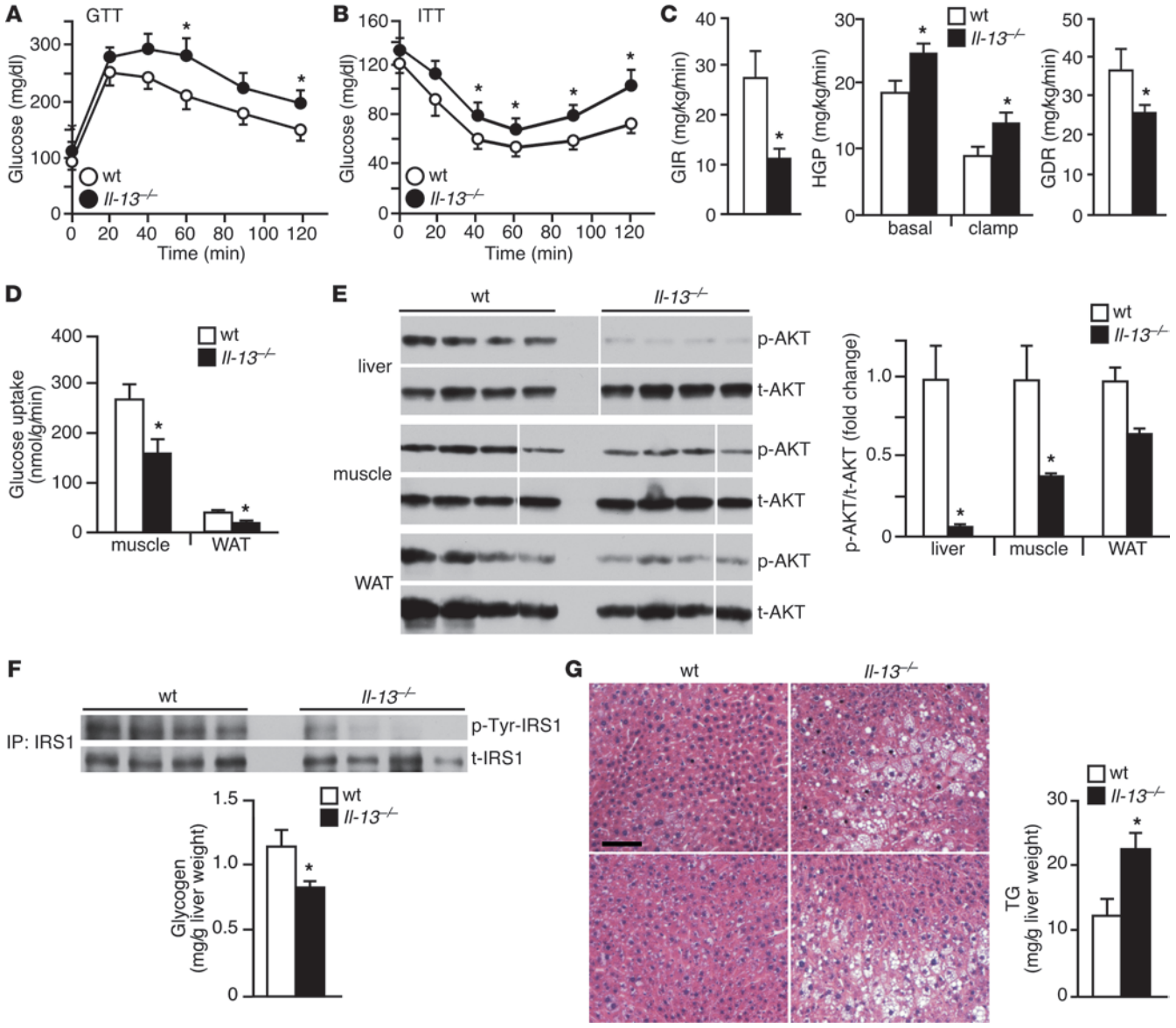

Figure 2

Il-13$^{-/-}$ mice develop hepatic insulin resistance and systemic metabolic dysfunction on normal chow. (**A** and **B**) GTT (**A**) and ITT (**B**) of 7- to 8-month-old chow-fed WT and *Il-13*$^{-/-}$ mice (C57BL/6 background; n = 7–10 per genotype). (**C**) Euglycemic-hyperinsulinemic clamp demonstrated that *Il-13*$^{-/-}$ mice were more insulin resistant than WT controls. GIR, glucose infusion rate; HGP, hepatic glucose production (basal and during clamp); GDR, glucose disposal rate. (**D**) Following the clamp, WT and *Il-13*$^{-/-}$ mice were given 2-deoxy-d-[1-^{14}C]glucose to determine tissue glucose uptake. (**E**) Immunoblotting of tissue insulin signaling, assessed by insulin-stimulated AKT phosphorylation. Liver, muscle, and WAT were collected following the clamp. Representative tissue samples from 4 individual mice are shown. Samples of the same tissue were run on the same gel but were noncontiguous (white lines). Quantification of immunoblot is also shown. t-AKT, total AKT. (**F**) Immunoblotting showed insulin-stimulated IRS1 tyrosine phosphorylation in the liver. Quantification of hepatic glycogen content is also shown. (**G**) Liver histology was performed to assess fat accumulation; shown are sections from 2 representative mice. Scale bar: 100 μm. Quantification of hepatic TG content is also shown. Data are mean ± SEM. *P < 0.05 vs. WT.

to the natural fasting and feeding states, respectively), which demonstrated that glucose concentrations of C57BL/6 *Il-13*$^{-/-}$ mice were also elevated during the fed state, when lactate production was reduced (10 PM; Figure 1D). Insulin concentrations during the fasted state (10 AM) were increased. In addition, C57BL/6 *Il-13*$^{-/-}$ mice exhibited higher circulating TG levels, but normal FFA and cholesterol levels (Figure 1E).

The increase in blood glucose and insulin levels indicated that *Il-13* depletion causes dysregulated glucose metabolism. In fact, glucose tolerance test (GTT) and insulin tolerance test (ITT) showed that C57BL/6 *Il-13*$^{-/-}$ mice were glucose intolerant and had reduced insulin sensitivity compared with control mice (Figure 2, A and B). Euglycemic-hyperinsulinemic clamp was performed to further characterize the defect in glucose homeostasis.

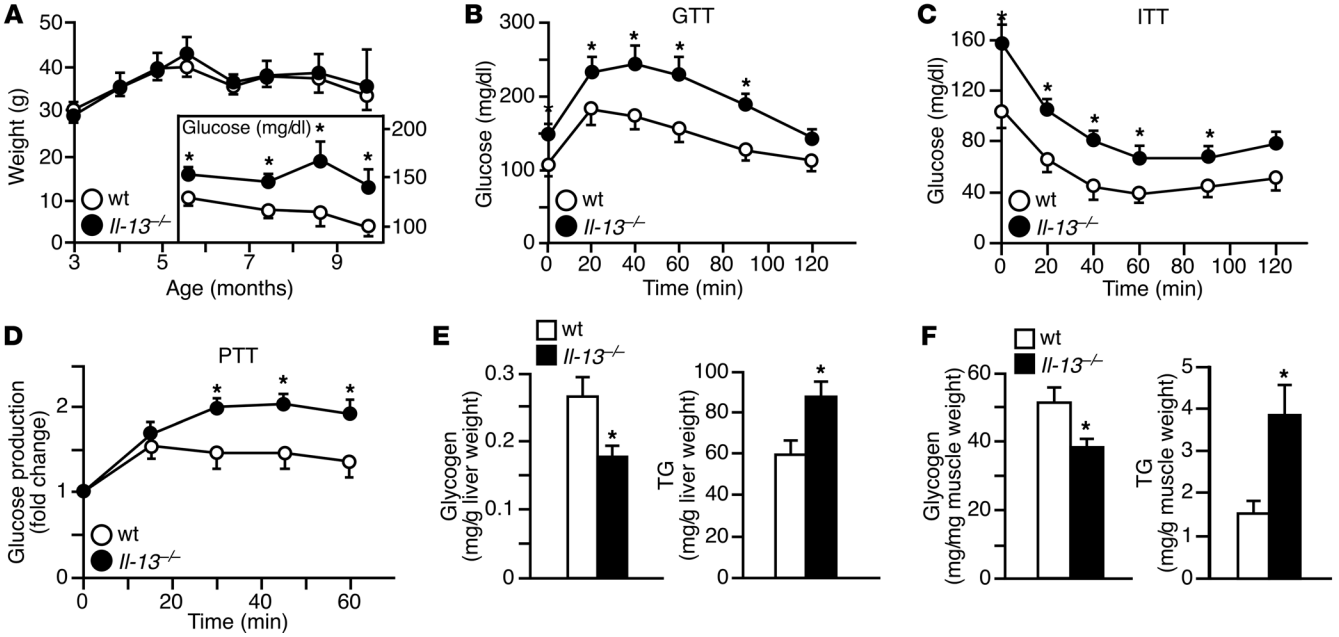

Figure 3

Hyperglycemia and increased hepatic glucose production in high-fat diet–fed BALB/c *Il-13*$^{-/-}$ mice. (**A**) WT and *Il-13*$^{-/-}$ mice (BALB/c background; $n = 8$ per genotype) were fed high-fat diet for 6 months. Body weight and blood glucose (inset) were measured at the indicated time points. (**B**) GTT. (**C**) ITT. (**D**) PTT showed increased glucose production in *Il-13*$^{-/-}$ mice. (**E** and **F**) Decreased glycogen and increased TG content in liver (**E**) and muscle (**F**) of *Il-13*$^{-/-}$ mice. Data are mean ± SEM. *$P < 0.05$ vs. WT.

C57BL/6 *Il-13*$^{-/-}$ mice required less exogenous glucose to maintain euglycemia (as demonstrated by a reduced glucose infusion rate), due to their increased hepatic glucose production — both at the basal level and during the clamp — and reduced glucose disposal (Figure 2C). Furthermore, glucose uptake was decreased in both muscle and WAT (Figure 2D). Tissue-specific insulin signaling was assessed by insulin-stimulated AKT phosphorylation. C57BL/6 *Il-13*$^{-/-}$ muscle and WAT showed decreased levels of phosphorylated AKT (p-AKT) compared with control animals (Figure 2E). The strongest reduction in p-AKT was observed in C57BL/6 *Il-13*$^{-/-}$ livers, where glycogen content and insulin-induced tyrosine phosphorylation of IRS1 were also lower, while fat accumulation was elevated (Figure 2, F and G). These observations suggest that C57BL/6 *Il-13*$^{-/-}$ mice exhibit systemic metabolic dysregulation with severe hepatic insulin resistance.

BALB/c Il-13$^{-/-}$ *mice develop hyperglycemia on high-fat diet.* We next sought to determine the effect of *Il-13* deficiency in the BALB/c genetic background. BALB/c mice exhibit a much stronger Th2 response (accompanied by a weak Th1 response) and are less prone to develop metabolic diseases than are C57BL/6 mice (31, 32). Chow-fed BALB/c *Il-13*$^{-/-}$ mice had normal body weight and glucose metabolism up to 6 months of age (Supplemental Figure 1, B and C). On high-fat diet (35% fat), BALB/c *Il-13*$^{-/-}$ mice had elevated concentrations of fasting glucose and TG, whereas weight gain and fasting insulin remained similar to those of control animals (Figure 3A and Supplemental Table 1). Elevated glucose concentrations were evident throughout the 2-hour period of both GTT and ITT (Figure 3, B and C). Pyruvate tolerance test (PTT) demonstrated that BALB/c *Il-13*$^{-/-}$ mice also exhibited increased hepatic glucose production (Figure 3D). Consistent with the dysregulated glucose metabolism, glycogen content was decreased, whereas TG content was increased, in both liver and muscle of BALB/c *Il-13*$^{-/-}$ mice (Figure 3, E and F). Notably, tissue insulin signaling, as assessed by insulin-stimulated p-AKT, appeared to be similar between high-fat diet–fed control and *Il-13*$^{-/-}$ mice (Supplemental Figure 1D). Collectively, our results from *Il-13*$^{-/-}$ mice in both genetic backgrounds implicated a critical role for IL-13 in maintaining glucose homeostasis.

Il-13 regulates hepatic gluconeogenesis. Insulin is known to suppress glucose output in the liver. The increased glucose production in C57BL/6 *Il-13*$^{-/-}$ mice (Figure 2) could be due to hepatic insulin resistance. To assess the physiological function of IL-13, pathways involved in glucose synthesis and production were examined in chow-fed C57BL/6 WT and *Il-13*$^{-/-}$ mice at 2 months of age, when insulin responsiveness (as determined by ITT) and circulating concentrations of fasting glucose, insulin, lactate, and lipids were similar between genotypes (data not shown). Liver samples were collected at 10 AM and 10 PM to examine fasting and feeding metabolic responses. Gluconeogenic gene expression at 10 AM was similar between the 2 C57BL/6 genotypes. As expected, mRNA levels of hepatic gluconeogenic genes (e.g., *Pcx*, *Fbp1*, and *G6p*) were decreased during the fed state (10 PM) compared with the fasted state (10 AM) in WT mice (Figure 4A). However, this downregulation was blunted in C57BL/6 *Il-13*$^{-/-}$ mice, concomitant with an increase in feeding blood glucose levels (WT, 176.07 ± 2.40 mg/dl glucose, *Il-13*$^{-/-}$, 188.66 ± 4.57 mg/dl glucose, $P < 0.05$; WT, 1.62 ± 0.37 ng/ml insulin, *Il-13*$^{-/-}$, 1.70 ± 0.44 ng/ml insulin). Induction of de novo lipogenic genes (e.g., *Srebp-1c* and acetyl-CoA carboxylase 1 and 2 [*Acc1/2*]) by feeding was not affected, consistent with the notion that C57BL/6 *Il-13*$^{-/-}$ mice at this age show a normal hepatic insulin response. Dysregulated glucose metabolism at the fed state worsened by 7 months of age, as demonstrated by increased expression of several gluconeogenic genes, including *Pcx*, *Pepck*,

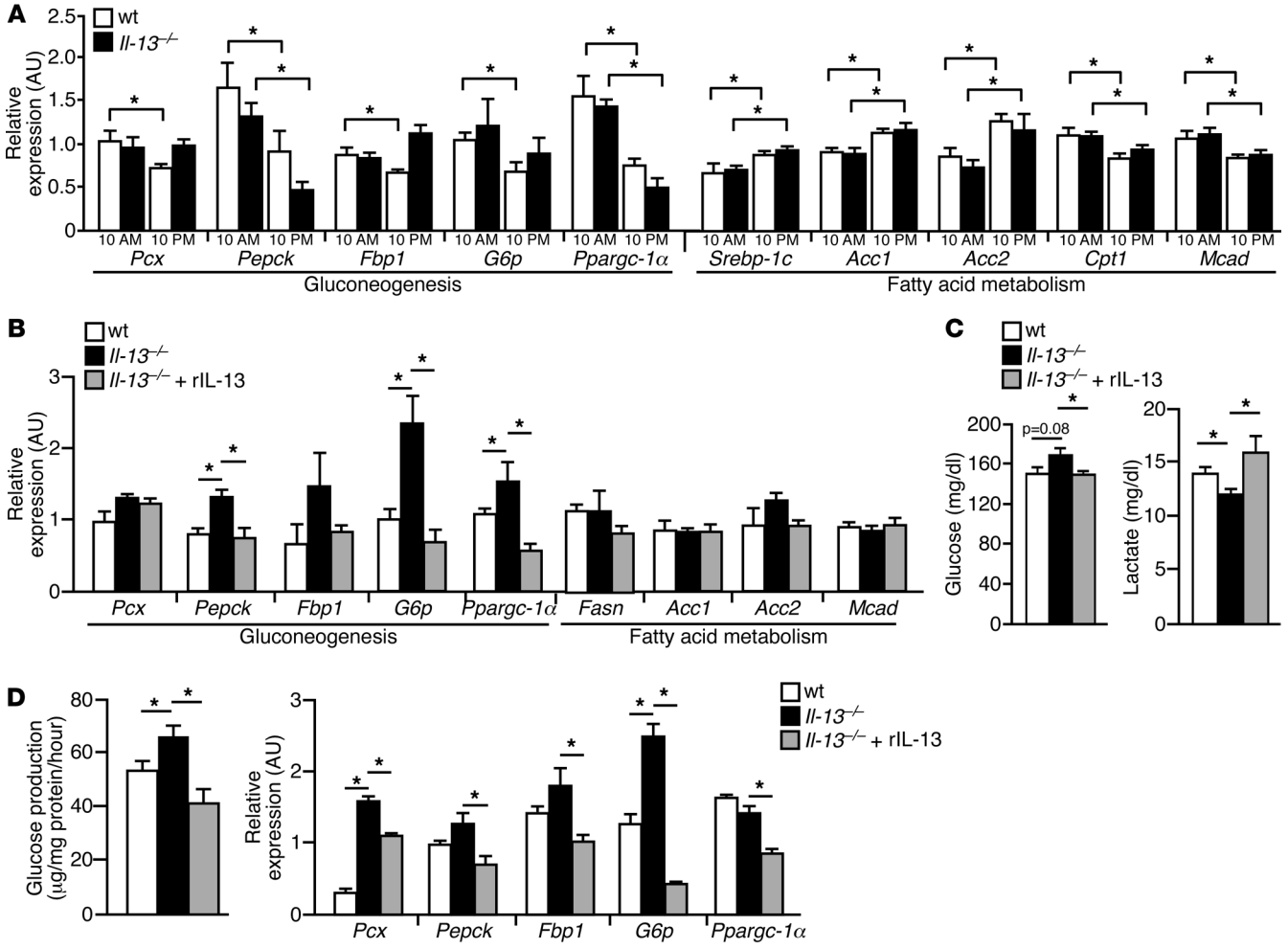

Figure 4

Dysregulation of hepatic gluconeogenic genes in *Il-13*$^{-/-}$ mice. (**A**) The effect of feeding-induced suppression on gluconeogenic gene expression was blunted in *Il-13*$^{-/-}$ mice. Livers from 2-month-old chow-fed WT and *Il-13*$^{-/-}$ mice (C57BL/6 background; $n = 6$ per genotype) were collected at 10 AM and 10 PM, and gene expression was examined by quantitative real-time PCR. (**B**) By 7 months of age, expression of the gluconeogenic pathway was further elevated in liver of chow-fed *Il-13*$^{-/-}$ mice (C57BL/6 background), which was normalized by rIL-13 injection (1 μg every other day, total 3 doses). Livers were collected at 10 PM. (**C**) Acute rIL-13 treatment rescued the glucose phenotype of *Il-13*$^{-/-}$ mice (cohort as in **B**). Blood glucose and lactate were measured at 10 PM. (**D**) Glucose production and gluconeogenic gene expression in primary hepatocytes derived from 4- to 5-month-old *Il-13*$^{-/-}$ mice. rIL-13 (10 ng/ml) was given to hepatocytes for 2 hours followed by a 4-hour glucose production assay in the presence of rIL-13. RNA was isolated 6 hours after rIL-13 treatment. Data are mean ± SEM. *$P < 0.05$.

Fbp1, *G6p*, and *Ppargc1α*, in C57BL/6 *Il-13*$^{-/-}$ mice (Figure 4B). Subsequently, recombinant IL-13 (rIL-13; 1 μg every other day, total 3 doses) was used to identify primary metabolic targets. rIL-13 treatment normalized gluconeogenic gene expression, but did not affect fatty acid metabolism genes, in C57BL/6 *Il-13*$^{-/-}$ mice (Figure 4B). rIL-13 also restored glucose and lactate to control levels (Figure 4C), suggesting a direct role for IL-13 in the control of hepatic glucose metabolism. Indeed, primary hepatocytes isolated from C57BL/6 *Il-13*$^{-/-}$ mice showed increased glucose production and gluconeogenic gene expression, a defect that was rescued by rIL-13 treatment for 6 hours (Figure 4D). Similar results were observed in livers/hepatocytes derived from high-fat diet–fed BALB/c *Il-13*$^{-/-}$ mice (Supplemental Figure 2, A and B). These data suggest that IL-13 depletion results in loss of postprandial glycemic control, leading to hepatic insulin resistance and fasting hyperglycemia.

Th2 cytokines have been shown to modulate high-fat diet–induced tissue inflammation (10) and brown adipose tissue (BAT) thermogenesis (33), both of which contribute to metabolic homeostasis. On normal chow, the expression of proinflammatory (M1) and antiinflammatory (M2) markers in the liver and WAT was similar between WT and *Il-13*$^{-/-}$ mice on the C57BL/6 background (Figure 5A). FACS and gene expression analyses showed same percentage of F4/80$^+$ cells (e.g., macrophages) with similar M1/M2 expression patterns in the liver and WAT of C57BL/6 *Il-13*$^{-/-}$ and WT mice (Supplemental Figure 3, A and B). The expression of 2 M2 genes, *Mgl1* and *Mrc1*, was lower by 20% in F4/80$^+$ cells from WAT of C57BL/6 *Il-13*$^{-/-}$ mice, but the protein levels were not significantly altered (Supplemental Figure 3, A and B). There was also no difference in concentrations of circulating cytokines/chemokines (TNF-α, IL-1β, MCP-1,

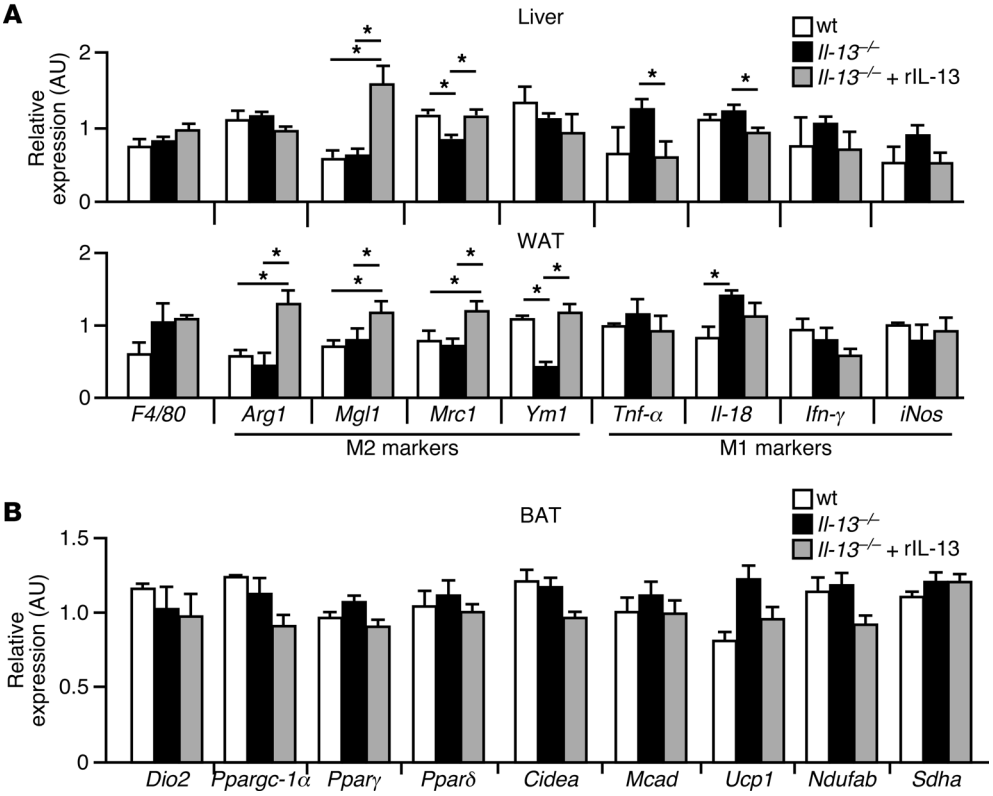

Figure 5
Minimal contribution of tissue inflammation to the metabolic phenotype of chow-fed *Il-13*$^{-/-}$ mice. (**A**) Expression profiling of inflammatory genes in liver and WAT from 7-month-old chow-fed WT, *Il-13*$^{-/-}$, and rIL-13–injected *Il-13*$^{-/-}$ mice (C57BL/6 background; cohort as in Figure 4B). *F4/80* is a macrophage marker. M1 and M2 markers represent classic (proinflammatory) and alternative (antiinflammatory) activation of macrophages, respectively. (**B**) Expression profiling of oxidative metabolism and thermogenic genes in BAT using real-time PCR. Data are mean ± SEM. *$P < 0.05$.

and MIP-3α) between genotypes (Supplemental Figure 3C). rIL-13 treatment was able to induce M2 genes (Figure 5A). These results were consistent with the notion that tissue inflammation is more relevant under conditions such as high-fat feeding and obesity (34–36). In fact, immune cell infiltration, typically identified by crown-like structures, was not evident based on WAT histology in these chow-fed C57BL/6 mice (Supplemental Figure 3D). In BAT, the mRNA levels of genes involved in mitochondrial oxidative metabolism and thermogenesis were not affected by IL-13 status (Figure 5B). *Il-13* gene deletion in the BALB/c background on high-fat diet led to downregulation of M2 markers, particularly in WAT (Supplemental Figure 4, A and B). Notably, proinflammatory genes were unchanged. There was no difference in BAT metabolic gene expression (Supplemental Figure 4C). Collectively, these results indicate that the defect in glucose metabolism in *Il-13*$^{-/-}$ mice under these experimental settings is mediated primarily by the function of IL-13 in hepatic gluconeogenic gene expression.

Stat3 mediates the suppressive effect on gluconeogenic gene expression by Il-13. Th2 signaling is known to induce phosphorylation and nuclear translocation of STAT6 to control transcription of M2 genes in immune cells (16). However, STAT3, another member of the STAT family known to suppress gluconeogenic genes (7, 8), has also been shown to interact with IL-13Rα1 (37, 38). Additionally, feeding is thought to increase p-STAT3 (39). We found that expression of *Il-13*, but not *Il-4*, was increased in the liver from fed compared with fasted mice (Supplemental Figure 5A). As reported above, p-STAT3 was readily detectable in WT liver at the fed state (10 PM). In contrast, levels of p-STAT3 were reduced in the liver of C57BL/6 *Il-13*$^{-/-}$ mice, which could be restored by rIL-13 treatment (Figure 6A). The p-STAT6 signal was relatively low in both genotypes, but inducible by rIL-13. To demonstrate a causal relationship between IL-13 and glucose production and identify the downstream mediators, we conducted functional studies in isolated hepatocytes using various genetic models. In primary hepatocytes, rIL-13 treatment led to rapid STAT3 phosphorylation (Figure 6B), which suggests that STAT3 may serve as an effector of IL-13 in regulating gluconeogenesis. In fact, the inhibitory effect of IL-13 on basal glucose production and gluconeogenic gene expression was abolished in *Stat3*$^{-/-}$ hepatocytes (with the exception of *Ppargc1α* expression), but was preserved in WT and *Stat6*$^{-/-}$ cells (Figure 6, C and D). In addition, rIL-13 was unable to suppress the activity of a reporter driven by a 1.7-kb PEPCK promoter element in *Stat3*$^{-/-}$ hepatocytes (Figure 6E). Reexpression of STAT3 in these cells reduced the promoter activity by 50%, which was further decreased with rIL-13 treatment. ChIP assays further demonstrated that IL-13 increased STAT3 occupancy on *Pepck* and *G6p* gene promoters (binding sites located at approximately –1 kb and at –5 kb, respectively; Figure 6F). siRNA knockdown of *Il-13rα1* (or *Stat3*) also abrogated the ability of IL-13 to increase STAT3 phosphorylation, reduce glucose production, and suppress gluconeogenic gene expression (Figure 6, G and H). Knockout or knockdown of *Stat3*, *Stat6*, or *Il-13rα1* was shown to be specific (Supplemental Figure 5, B and C). These findings demonstrated that IL-13 controls glucose homeostasis through the IL-13Rα1/STAT3 signaling pathway in the liver.

As mentioned above, many immune cells are capable of producing IL-13. To identify potential IL-13–producing cells within the liver, we first used *Il-13*^{eGFP} reporter mice, which contained a *GFP* knockin within the *Il-13* locus (25). T cells, type I NKT cells, B cells, and macrophages were readily detected in the liver by FACS, whereas the presence of eosinophils and Lin$^-$ICOS$^+$Sca-1$^+$CD25$^+$IL-7Rα$^+$

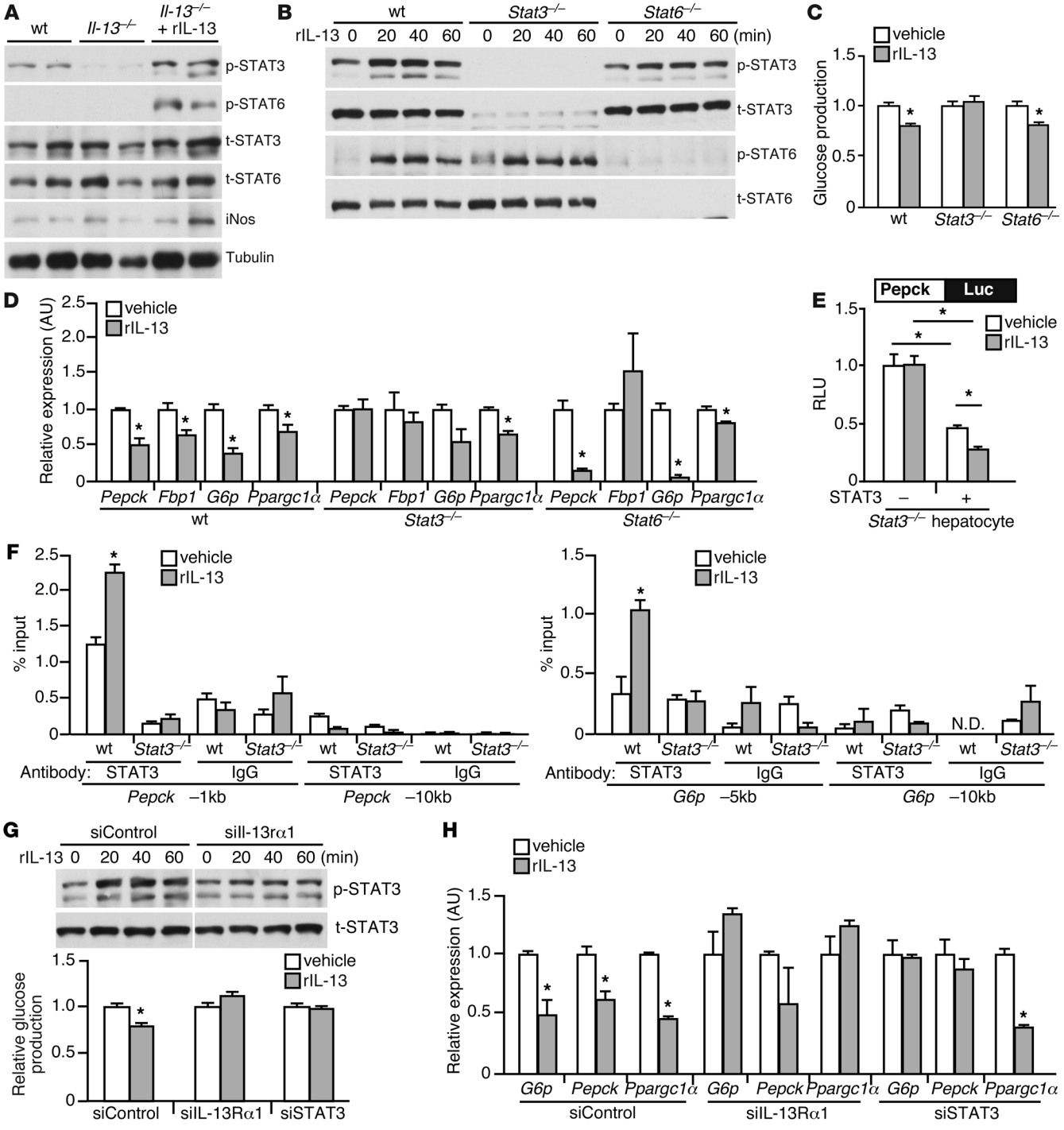

Figure 6

IL-13 suppresses gluconeogenic gene expression through STAT3. (**A**) Immunoblotting showing reduced p-STAT3 levels in *Il-13*$^{-/-}$ liver. Liver samples were collected at 10 PM (2 representative mice per group; cohort as in Figure 4B). (**B**) Immunoblotting showed that IL-13 induced STAT3/STAT6 phosphorylation in primary hepatocytes from WT, liver-specific *Stat3*$^{-/-}$, and *Stat6*$^{-/-}$ mice. (**C**) IL-13 suppressed glucose production in hepatocytes in a STAT3-dependent manner. (**D**) IL-13 decreased expression of gluconeogenic genes through STAT3. Samples were collected 6 hours after rIL-13 treatment for gene expression analyses by quantitative real-time PCR. (**E**) Suppression of PEPCK promoter activity by IL-13 was mediated by STAT3. *Stat3*$^{-/-}$ hepatocytes were transfected with a luciferase reporter driven by PEPCK promoter, STAT3 expression vector, and/or rIL-13. RLU, relative luciferase unit. (**F**) ChIP in WT and *Stat3*$^{-/-}$ hepatocytes showed STAT3 occupancy on *Pepck* and *G6p* promoters induced by IL-13. ND, not detected. (**G**) IL-13Rα1 was required for IL-13–dependent inhibition of glucose production. Hepatocytes were isolated from WT mice and transfected with siRNAs targeting either *Il-13rα1* (siIL-13Rα1) or *Stat3* (siSTAT3). siControl, control siRNA. Immunoblotting of p-STAT3 and total STAT3 in hepatocytes transfected with control or IL-13Rα1 siRNA is also shown. Samples were run on the same gel but were noncontiguous (white lines). (**H**) IL-13Rα1 mediated IL-13–dependent inhibition on gluconeogenic gene expression, as assessed by quantitative real-time PCR. Glucose production and gene expression are presented as fold change relative to control. Data are mean ± SEM. **P* < 0.05 vs. vehicle, or as indicated by brackets.

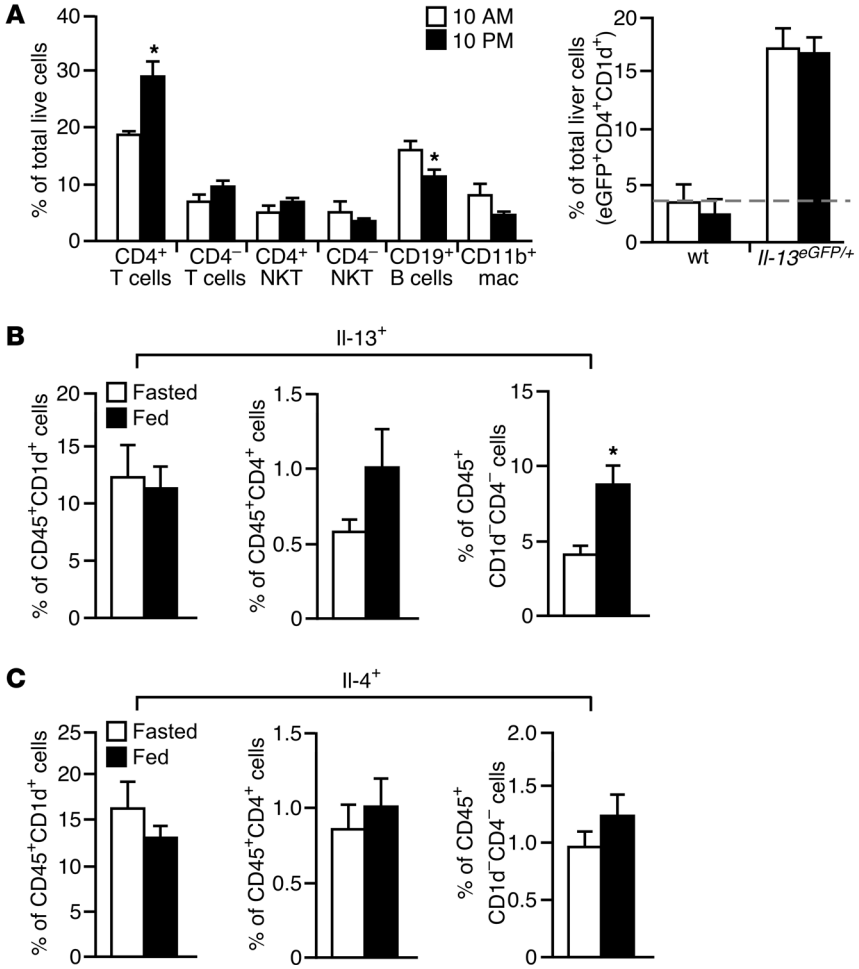

Figure 7
Assessment of IL-13–producing cells in the liver. (**A**) Immune cell populations in the liver collected at 10 AM and 10 PM, determined by FACS. mac, macrophages. Detection of IL-13$^+$ NKT cells using *Il-13^{eGFP}* is also shown. Dotted line indicates the background signal in WT BALB/c cells (n = 3–4 per time point). (**B**) IL-13 and (**C**) IL-4 expression in CD1d$^+$ NKT cells, CD4$^+$ T cells, and CD1d$^-$CD4$^-$ cells, determined by FACS. Liver CD45$^+$ immune cells were isolated from mice (n = 4 per group) that were fasted overnight or refed for 2 hours. Data are mean ± SEM. *P < 0.05.

nuocytes (an ILC2 cell type) was not evident (Figure 7A and data not shown). There was an increase in the percentage of CD4$^+$ T cells and a decrease in CD19$^+$ B cells at the fed state. However, the main IL-13$^+$ population identified using *Il-13$^{eGFP/+}$* mice appeared to be in CD4$^+$ NKT cells (Figure 7A), at both fed (10 PM) and fasted (10 AM) states. We also determined IL-13 expression in CD45$^+$ liver immune cells. Similarly, a higher percentage of type I NKT cells was found to be IL-13$^+$. Of note, in CD45$^+$CD4$^-$CD1d$^-$ (non-T, non-NKT) cells, the IL-13$^+$ population from the fed state was higher than that from the fasted state (Figure 7B). In contrast, there was no difference in IL-4$^+$ population (Figure 7C). These results suggest that although NKT cells represent a major source of IL-13 in the liver, certain non-T, non-NKT cells may also contribute to IL-13 release in response to feeding.

Discussion

The metabolic benefit of Th2 cytokines is believed to resolve, at least in part, the proinflammatory response elicited by Th1 signaling that has been shown to inhibit insulin sensitivity. Using experimental conditions that minimize contributions from metabolic stress–induced inflammation, the current study identified a key function for IL-13 in hepatic glucose production. Depletion of *Il-13* by gene targeting resulted in hyperglycemia accompanied by elevated expression of genes required for glucose synthesis and production in the liver, while rIL-13 treatment reversed the dysregulated glucose metabolism. In the C57BL/6 background, the hyperglycemic phenotype of chow fed *Il-13$^{-/-}$* mice worsened with age, leading to hepatic and systemic insulin resistance. BALB/c *Il-13$^{-/-}$* mice also showed elevated glucose levels with high-fat diet feeding. IL-13 suppressed transcription of gluconeogenic genes through a noncanonical downstream transcription factor, STAT3, and the effect of IL-13 on inhibition of glucose production was lost in *Stat3$^{-/-}$* hepatocytes. These results suggest that IL-13 exhibits metabolic functions beyond its role in modulating inflammation.

In response to endotoxin, the body exhibits transient systemic insulin resistance, in an attempt to spare glucose for utilization by immune cells (40–42). It is therefore conceivable that in addition to resolving inflammation, one of the main functions of IL-13 is to restore glucose homeostasis that is disrupted by proinflammatory actions. Along this line, nutrient intake may trigger low-grade inflammation through mechanisms including O-GlcNAcylation–mediated activation of NF-κB, as described previously (13). In healthy individuals, insulin is necessary and sufficient to quickly restore glucose levels after feeding. IL-13 is likely required when insulin signaling is compromised or overwhelmed, such as in aged individuals or in cases of overnutrition. Although the glucose-lowering effect of IL-13 may help keep metabolic inflammation under control, this activity is independent of its function in macrophage polarization. Increased circulating glucose levels were observed in C57BL/6 *Il-13$^{-/-}$* mice on normal chow, which did not elicit strong tissue inflammation. In the BALB/c background, a strain resistant to metabolic diseases (32), hyperglycemia in *Il-13$^{-/-}$* mice was brought about by high-fat diet feeding without altering insulin sensitivity. In line with IL-13's role in macrophage alternative activation, the expression of WAT M2 genes was reduced. However, proinflammatory markers were not altered. This is not unexpected, because BALB/c mice are known to have a weaker M1 response (31). Our results from these 2 mouse models indicated that the M1/M2 paradigm could be extended to direct metabolic control, in which M1 causes dysregulated glucose metabolism by inhibiting insulin signaling, while M2 (notably IL-13) maintains glucose homeostasis by suppressing hepatic glucose production.

STAT6 is known as the main effector of Th2 cytokines in immune cells (16, 43). In fact, IL-4/STAT6 signaling is essential for Th2 cell differentiation (44–46). STAT6 has also been shown to mediate certain physiological functions of IL-4, most notably adaptive thermogenesis in BAT (33). In contrast, IL-13 was not required for Th2 differentiation nor thermogenic gene expression (Figure 5B and Supplemental Figure 4C). Interestingly, IL-4 did not appear to control hepatic gluconeogenesis (Supplemental Figure 5D). It is unclear how the differential activities of Th2 cytokines are regulated, as both IL-4 and IL-13 can signal through the type II receptor IL-13Rα1/IL-4Rα heterodimer (30). Structure-based studies suggest that the relative expression of IL-4Rα and IL-13Rα1 may determine the outputs of IL-4 versus IL-13 signaling (30). Although early studies established an interaction between STAT3 and the IL-13Rα1 subunit (37, 38), Th2 cytokines have been shown to weakly activate STAT3 in immune cell lines (30, 38). The ability of IL-13 to induce STAT3 phosphorylation in primary hepatocytes appeared to be rapid and robust (Figure 6), consistent with relatively high expression of IL-13Rα1 in hepatocytes compared with adipocytes and T cells (Supplemental Figure 1A). Levels of p-STAT3 in the liver have been shown to be increased by feeding, although the upstream signaling is not clear (39). Together, these observations suggest that the IL-13/STAT3 axis directs Th2 signaling toward metabolic responses, such as feeding, whereas IL-4 and STAT6 may play roles in adaptive responses. This notion is supported by recent work that identified widely dispersed IL-13–producing cells characterized as non-T, non-B, lineage-negative ILC2 cells that did not express IL-4 (24–26, 29). These cells provide early sources of IL-13 during helminth infection, whereas T cell–derived Th2 cytokines are thought to be important for the development of adaptive immunity (47). NKT cells represent another innate cell type capable of producing IL-13. Our data suggest that type I NKT cells are a main source of IL-13 in the liver. Although this cell population is not altered by feeding, a recent study demonstrated that NKT cell activation can be modulated by dietary fats (28). In addition to NKT cells, a population of non-T, non-NKT cells isolated from livers of fed mice expressed higher IL-13 levels than did the same population in fasted animals. These cells were also low in IL-4 and thus appeared to exhibit certain characteristics of ILC2 cells. We did not detect nuocytes, but other ILC2 populations may be involved, such as Ih2 and natural helper cells expressing different markers or MPP^{type2} cells (48, 49). Collectively, these observations suggest that metabolic stress is sensed by multiple innate immune cells, which may help maintain metabolic homeostasis via release of IL-13.

STAT3 has previously been shown to be recruited to promoters of *G6p* and *Pepck* in response to IL-6 (8), but the mechanism by which STAT3 actively represses transcription remains unclear. The role of IL-6 in glucose metabolism and metabolic homeostasis is complex. As a result, genetic models of *Il-6* deletion have yielded conflicting metabolic phenotypes (50–53). Our current results demonstrated that IL-13 is a physiological signal that activates hepatic STAT3 to suppress glucose production. Our data also showed that depletion of IL-13 leads to hyperglycemia, which progresses to hepatic and systemic insulin resistance. Importantly, the ability of IL-13 to reduce glucose production appears to be independent of insulin signaling. Although the data presented here indicate the liver as a major site of IL-13 action (in addition to macrophages), we could not rule out the possibility that IL-13 targets other metabolic tissues. In addition, *Il-13*$^{-/-}$ mice in both genetic backgrounds had higher hepatic fat accumulation than did control animals. IL-13 does not affect the expression of hepatic genes involved in fatty acid synthesis and catabolism. In primary hepatocytes, rIL-13 treatment reduced lipogenesis and increased fatty acid oxidation in *Il-13*$^{-/-}$, but not WT, cells (Supplemental Figure 5E). It is possible that the hepatic steatosis phenotype of *Il-13*$^{-/-}$ mice is secondary to the lower metabolic rate and metabolic dysregulation. Nevertheless, the IL-13/STAT3 pathway in the liver may provide new therapeutic opportunities to control hyperglycemia associated with insulin resistance.

Methods

Animals and metabolic studies. *Il-13*$^{-/-}$ mice in the BALB/c background were generated as described previously (54). These animals were backcrossed 5 generations to the C57BL/6 strain (96.875%). Background- and age-matched littermates (males) were used as WT controls. Metabolic studies in chow-fed C57BL/6 WT and *Il-13*$^{-/-}$ mice were conducted in 4 cohorts (n = 6–10 per genotype, 2–9 months of age). For high-fat diet–fed BALB/c *Il-13*$^{-/-}$ mice (n = 8 per genotype; 2 cohorts), 10- to 12-week-old mice were placed on a high-fat diet (Bio-Serv) for 6 months. WT and BALB/c *Il-13*$^{-/-}$ mice (n = 5 per genotype, 4–6 months of age; 2 cohorts) fed normal chow were also studied. ITT and GTT were performed as described previously (55) using 1 U/kg body weight insulin and 1.5 g/kg glucose, respectively, by i.p. injection after a 6-hour fast. For PTT, mice were fasted for 16 hours followed by i.p. injection of sodium pyruvate (2 g/kg). Blood glucose concentrations were measured at the indicated time points using a glucometer (OneTouch Ultra; LifeScan). Fasting blood chemistries, including TGs, FFAs, cholesterol, and lactate, were measured following a 6-hour fast using commercial kits (Wako, Themo-Fisher). In certain experiments, blood chemistries, serum cytokines/chemokines, and tissue samples were determined at 10 AM and 10 PM, corresponding to the natural fasting and feeding states, respectively. These mice were fed ad libitum and housed in a quiet room without disturbance of their sleep/wake behavior to reduce environmental stress. Serum cytokines were measured using Luminex multiplex kits (Millipore). Quantification of liver and muscle TGs and glycogen was based on published protocols (56). Metabolic cage studies and DEXA were performed as described previously (55). For in vivo rescue studies, mice were given either 1 μg rIL-13 (Peprotech) or an equal volume of PBS every other day for 1 week (total 3 doses; n = 5 per treatment). *Stat6*$^{-/-}$ mice (C57BL/6 background) were purchased from the Jackson Laboratory. Liver-specific *Stat3*$^{-/-}$ mice were generated as described previously (7) and provided by J. Mizgerd (Boston University, Boston, Massachusetts, USA). Mice were housed in the Harvard School of Public Health barrier facility on a 12-hour light, 12-hour dark cycle.

Euglycemic-hyperinsulinemic clamp. Mice were implanted with catheters followed by a 5-day recovery (57). After an initial 5-μCi bolus, [3-^{3}H]glucose was infused (0.05 μCi/min for 2 hours) to measure basal glucose turnover. A 2-hour euglycemic-hyperinsulinemic clamp was conducted with a prime and continuous insulin infusion (2.5 mU/kg/min), coupled with a variable infusion of 40% glucose to maintain blood glucose at 6 mM. Every 5 minutes, blood glucose was measured via tail bleed during the first hour to stabilize blood glucose levels and every 10 minutes thereafter until the end of the 2-hour clamp to maintain constant blood glucose levels. The rate of whole-body glucose turnover was estimated using a continuous infusion of [3-^{3}H]glucose (0.1 μCi/min). Tissue-specific glucose uptake was estimated by a bolus administration of 2-deoxy-d-[1-^{14}C]glucose (10 μCi) 45 minutes prior to the end of clamp experiments.

Primary hepatocytes and glucose production assays. Primary hepatocytes were isolated and cultured as described previously (56) using Liberase (Roche) from WT, *Il-13*$^{-/-}$, *Stat6*$^{-/-}$, and liver-specific *Stat3*$^{-/-}$ mice. To measure glu-

cose production, hepatocytes were treated with rIL-13 (10 ng/ml) or vehicle in DMEM low-glucose media for 2 hours, washed, and incubated for 4 hours in glucose production media (DMEM without glucose or phenol red, supplemented with 1 mM pyruvate, 10 mM lactate, and 10 ng/ml rIL-13). Glucose concentrations in the media were measured enzymatically and normalized to total protein content. For siRNA experiments, hepatocytes seeded in 12-well plates were transfected with 40 pmol siRNA pools (Qiagen) using Lipofectamine 2000 (Invitrogen) for 48 hours, followed by glucose production assays.

Reporter assays and ChIP. For reporter assays, a 1.7-kb mouse PEPCK promoter element was cloned into the pGL3-basic vector. Hepatocytes were transfected with the promoter construct together with CMV-STAT3 or empty vector followed by overnight treatment with rIL-13. The relative luciferase unit was normalized using the dual-luciferase reporter assay system (Promega). For ChIP, 8×10^7 WT and *Stat3*$^{-/-}$ hepatocytes were plated onto 15-cm plates and treated with rIL-13 overnight. Samples were harvested and processed using the SimpleChIP chromatin immunoprecipitation kit (Cell Signaling). STAT3 antibody and IgG control were from Cell Signaling. Real-time PCR was performed to determine STAT3 occupancy using primers flanking putative STAT3 binding sites on the promoters of *Pepck* (approximately –1 kb relative to the transcription initial site) and *G6p* (approximately –5 kb) (8) as well as off-target sites (–10 kb) for each promoter. The following primers were used: *Pepck* –1 kb forward, 5′-GTTGCTCAAGTGCCAC-3′; *Pepck* –1 kb reverse, 5′-GTAGACCCTTCAGTGTC-3′; *Pepck* –10 kb forward, 5′-CTGGTTGTAAGGTGGGGGTC-3′; *Pepck* –10 kb reverse, 5′-GGAGAGCTCTGTGGTACAGC-3′; *G6p* –5 kb forward, 5′-GCTTGGTTGTGTGCTTTGCCTAGC-3′; *G6p* –5 kb reverse, 5′-GCTGACCTTAAATTCTCTCTGTAGCC-3′; *G6p* –10 kb forward, 5′-GAATCCAGTCAGTGTGACCTAGG-3′; *G6p* –10 kb reverse, 5′-GTGTCTGAAGACAGCTACAGTGTACTTAC-3′.

Gene expression. RNA was isolated from tissues (TRIzol) or cells (USB-Affymetrix) and reverse transcribed with random hexamer and oligo-dT primers (1:1 ratio). Relative gene expression was determined by SYBR green–based real-time PCR. Transcripts were normalized to *36B4* expression.

Immunoblotting. Cells and tissues were lysed in IP buffer (20 mM Tris HCl, pH 8.0; 100 mM NaCl; 1 mM EDTA; 0.1% NP-40; 10% glycerol; 1 mM DTT; and protease and phosphatase inhibitors). For IRS1 tyrosine phosphorylation, tissue samples were immunoprecipitated with anti-IRS1 antibody, followed by immunoblotting with anti–p-tyrosine and anti-IRS1 antibodies. Antibodies against the following proteins were used (all from Cell Signaling): p-AKT (pS473), AKT, IRS1, p-STAT3 (pY705), STAT3, p-STAT6 (pY641), STAT6, β-tubulin, and p-tyrosine (Cell Signaling). Anti-iNOS was from Santa Cruz Biotechnology.

Il-13–producing cells in the liver. To determine potential sources of IL-13, liver samples from ad libitum–fed WT BALB/c and *Il-13*$^{eGFP/+}$ mice (female, aged 6–8 weeks, backcrossed 11 generations to BALB/c) (25) were collected at 10 AM and 10 PM (n = 3–4 per genotype per time point). Hepatocytes were removed from the preparation through a 44% percoll gradient. FACS was performed to examine the presence of CD4$^+$ and CD8$^+$ T cells, CD19$^+$ B cells, and CD11b$^+$ macrophages as well as CD4$^+$ and CD4$^-$CD1d$^+$ NKT cells (25). Nuocytes (Lin$^-$ICOS$^+$Sca-1$^+$CD25$^+$IL-7Rα$^+$) and eosinophils (SiglecF$^+$) were not detected. Similar results were obtained from both genotypes, and the data were combined in Figure 7A. IL-13$^+$ cells in each cell population were further determined with GFP signal. A second approach was performed to identify IL-13$^+$ and IL-4$^+$ cells: liver immune cells from fasted or fed mice (8-week-old male C57BL/6; n = 4 per time point) were purified using percoll gradient and cultured in RPMI1640 culture medium (10% FBS, 50 μM 2-mercaptoethanol, and 2 mM glutamine) with 50 ng/ml phorbol myristate acetate (Sigma-Aldrich), 10 μg/ml brefeldin A (Invitrogen), and 10 μM monensin (Sigma-Aldrich) for 3 hours before FACS analyses using antibodies against CD45, CD4, CD1d, and IL-13 (28).

Statistics. Data are presented as mean ± SEM. Statistical differences between WT and *Il-13*$^{-/-}$ mice or between 10 AM and 10 PM were assessed using 2-tailed Student's t test. For in vitro assays, the mean and SEM were determined from 3–4 biological replicates for 1 representative experiment. Experiments were repeated at least 3 times. A P value less than 0.05 was considered significant.

Study approval. Animal studies were approved by the Harvard Medical Area Standing Committee on Animals.

Acknowledgments

The authors thank S.M. Reilly and U. Ünlütürk for technical assistance, S. Akira and K. Takeda (Osaka University, Osaka, Japan) for providing floxed *Stat3* mice, and G.S. Hotamisligil for help with metabolic cage and DEXA studies. P. Bhargava and K. Stanya were supported by NIH training grant T32ES016645. This work was supported by the American Heart Association, by the American Diabetes Association, and by NIH grant R01DK075046 (to C.H. Lee).

Received for publication May 22, 2012, and accepted in revised form October 4, 2012.

Address correspondence to: Chih-Hao Lee, Department of Genetics and Complex Diseases, Harvard School of Public Health, 665 Huntington Ave., Bldg. 1, Rm. 207, Boston, Massachusetts 02115, USA. Phone: 617.432.5778; Fax: 617.432.5236; E-mail: clee@hsph.harvard.edu.

Hang Shi's present address is: Department of Biology, Georgia State University, Atlanta, Georgia, USA.

1. Monnier L, Colette C, Dunseath GJ, Owens DR. The loss of postprandial glycemic control precedes stepwise deterioration of fasting with worsening diabetes. *Diabetes Care*. 2007;30(2):263–269.
2. Tahrani AA, Bailey CJ, Del Prato S, Barnett AH. Management of type 2 diabetes: new and future developments in treatment. *Lancet*. 2011;378(9786):182–197.
3. Chang-Chen KJ, Mullur R, Bernal-Mizrachi E. Beta-cell failure as a complication of diabetes. *Rev Endocr Metab Disord*. 2008;9(4):329–343.
4. Altarejos JY, Montminy M. CREB and the CRTC co-activators: sensors for hormonal and metabolic signals. *Nat Rev Mol Cell Biol*. 2011;12(3):141–151.
5. Lin HV, Accili D. Hormonal regulation of hepatic glucose production in health and disease. *Cell Metab*. 2011;14(1):9–19.
6. Cheng Z, White MF. The AKTion in non-canonical insulin signaling. *Nat Med*. 2012;18(3):351–353.
7. Inoue H, et al. Role of STAT-3 in regulation of hepatic gluconeogenic genes and carbohydrate metabolism in vivo. *Nat Med*. 2004;10(2):168–174.
8. Ramadoss P, Unger-Smith NE, Lam FS, Hollenberg AN. STAT3 targets the regulatory regions of gluconeogenic genes in vivo. *Mol Endocrinol*. 2009;23(6):827–837.
9. Lu M, et al. Insulin regulates liver metabolism in vivo in the absence of hepatic Akt and Foxo1. *Nat Med*. 2012;18(3):388–395.
10. Bhargava P, Lee CH. Role and function of macrophages in the metabolic syndrome. *Biochem J*. 2012;442(2):253–262.
11. Hotamisligil GS. Inflammation and metabolic disorders. *Nature*. 2006;444(7121):860–867.
12. Osborn O, Olefsky JM. The cellular and signaling networks linking the immune system and metabolism in disease. *Nat Med*. 2012;18(3):363–374.
13. Issad T, Kuo M. O-GlcNAc modification of transcription factors, glucose sensing and glucotoxicity. *Trends Endocrinol Metab*. 2008;19(10):380–389.
14. Arkan MC, et al. IKK-beta links inflammation to obesity-induced insulin resistance. *Nat Med*. 2005;11(2):191–198.
15. Cai D, et al. Local and systemic insulin resistance resulting from hepatic activation of IKK-beta and NF-kappaB. *Nat Med*. 2005;11(2):183–190.
16. Martinez FO, Helming L, Gordon S. Alternative activation of macrophages: an immunologic functional perspective. *Annu Rev Immunol*. 2009;27:451–483.
17. Kang K, et al. Adipocyte-derived Th2 cytokines and myeloid PPARdelta regulate macrophage polarization and insulin sensitivity. *Cell Metab*. 2008;7(6):485–495.
18. Odegaard JI, et al. Macrophage-specific PPARgamma controls alternative activation and improves insulin

resistance. *Nature*. 2007;447(7148):1116–1120.
19. Odegaard JI, et al. Alternative M2 activation of Kupffer cells by PPARdelta ameliorates obesity-induced insulin resistance. *Cell Metab*. 2008; 7(6):496–507.
20. Ricardo-Gonzalez RR, et al. IL-4/STAT6 immune axis regulates peripheral nutrient metabolism and insulin sensitivity. *Proc Natl Acad Sci U S A*. 2010;107(52):22617–22622.
21. Wu D, et al. Eosinophils sustain adipose alternatively activated macrophages associated with glucose homeostasis. *Science*. 2011;332(6026):243–247.
22. Chawla A, Nguyen KD, Goh YP. Macrophage-mediated inflammation in metabolic disease. *Nat Rev Immunol*. 2011;11(11):738–749.
23. Sun S, Ji Y, Kersten S, Qi L. Mechanisms of inflammatory responses in obese adipose tissue. *Annu Rev Nutr*. 2012;32:261–286.
24. Moro K, et al. Innate production of T(H)2 cytokines by adipose tissue-associated c-Kit(+)Sca-1(+) lymphoid cells. *Nature*. 2010;463(7280):540–544.
25. Neill DR, et al. Nuocytes represent a new innate effector leukocyte that mediates type-2 immunity. *Nature*. 2010;464(7293):1367–1370.
26. Price AE, et al. Systemically dispersed innate IL-13-expressing cells in type 2 immunity. *Proc Natl Acad Sci U S A*. 2010;107(25):11489–11494.
27. Winer S, et al. Normalization of obesity-associated insulin resistance through immunotherapy. *Nat Med*. 2009;15(8):921–929.
28. Ji Y, et al. Activation of natural killer T cells promotes M2 Macrophage polarization in adipose tissue and improves systemic glucose tolerance via interleukin-4 (IL-4)/STAT6 protein signaling axis in obesity. *J Biol Chem*. 2012;287(17):13561–13571.
29. Saenz SA, et al. IL25 elicits a multipotent progenitor cell population that promotes T(H)2 cytokine responses. *Nature*. 2010;464(7293):1362–1366.
30. LaPorte SL, et al. Molecular and structural basis of cytokine receptor pleiotropy in the interleukin-4/13 system. *Cell*. 2008;132(2):259–272.
31. Mills CD, Kincaid K, Alt JM, Heilman MJ, Hill AM. M-1/M-2 macrophages and the Th1/Th2 paradigm. *J Immunol*. 2000;164(12):6166–6173.
32. Nishikawa S, Yasoshima A, Doi K, Nakayama H, Uetsuka K. Involvement of sex, strain and age factors in high fat diet-induced obesity in C57BL/6J and BALB/cA mice. *Exp Anim*. 2007;56(4):263–272.
33. Nguyen KD, et al. Alternatively activated macrophages produce catecholamines to sustain adaptive thermogenesis. *Nature*. 2011;480(7375):104–108.
34. Lumeng CN, DelProposto JB, Westcott DJ, Saltiel AR. Phenotypic switching of adipose tissue macrophages with obesity is generated by spatiotemporal differences in macrophage subtypes. *Diabetes*. 2008;57(12):3239–3246.
35. Weisberg SP, McCann D, Desai M, Rosenbaum M, Leibel RL, Ferrante AW. Obesity is associated with macrophage accumulation in adipose tissue. *J Clin Invest*. 2003;112(12):1796–1808.
36. Xu H, et al. Chronic inflammation in fat plays a crucial role in the development of obesity-related insulin resistance. *J Clin Invest*. 2003;112(12):1821–1830.
37. Orchansky PL, Kwan R, Lee F, Schrader JW. Characterization of the cytoplasmic domain of interleukin-13 receptor-alpha. *J Biol Chem*. 1999;274(30):20818–20825.
38. Umeshita-Suyama R, et al. Characterization of IL-4 and IL-13 signals dependent on the human IL-13 receptor alpha chain 1: redundancy of requirement of tyrosine residue for STAT3 activation. *Int Immunol*. 2000;12(11):1499–1509.
39. Nie Y, et al. STAT3 inhibition of gluconeogenesis is downregulated by SirT1. *Nat Cell Biol*. 2009;11(4):492–500.
40. Agwunobi AO, Reid C, Maycock P, Little RA, Carlson GL. Insulin resistance and substrate utilization in human endotoxemia. *J Clin Endocrinol Metab*. 2000;85(10):3770–3778.
41. Virkamaki A, Yki-Jarvinen H. Mechanisms of insulin resistance during acute endotoxemia. *Endocrinology*. 1994;134(5):2072–2078.
42. Yki-Jarvinen H, Sammalkorpi K, Koivisto VA, Nikkila EA. Severity, duration, and mechanisms of insulin resistance during acute infections. *J Clin Endocrinol Metab*. 1989;69(2):317–323.
43. Gordon S. Alternative activation of macrophages. *Nat Rev Immunol*. 2003;3(1):23–35.
44. Kaplan MH, Schindler U, Smiley ST, Grusby MJ. Stat6 is required for mediating responses to IL-4 and for development of Th2 cells. *Immunity*. 1996;4(3):313–319.
45. Shimoda K, et al. Lack of IL-4-induced Th2 response and IgE class switching in mice with disrupted Stat6 gene. *Nature*. 1996;380(6575):630–633.
46. Takeda K, et al. Essential role of Stat6 in IL-4 signalling. *Nature*. 1996;380(6575):627–630.
47. Liang HE, Reinhardt RL, Bando JK, Sullivan BM, Ho IC, Locksley RM. Divergent expression patterns of IL-4 and IL-13 define unique functions in allergic immunity. *Nat Immunol*. 2011;13(1):58–66.
48. Neill DR, McKenzie AN. Nuocytes and beyond: new insights into helminth expulsion. *Trends Parasitol*. 2011;27(5):214–221.
49. Saenz SA, Noti M, Artis D. Innate immune cell populations function as initiators and effectors in Th2 cytokine responses. *Trends Immunol*. 2010; 31(11):407–413.
50. Clementi AH, Gaudy AM, Zimmers TA, Koniaris LG, Mooney RA. Deletion of interleukin-6 improves pyruvate tolerance without altering hepatic insulin signaling in the leptin receptor-deficient mouse. *Metabolism*. 2011;60(11):1610–1619.
51. Di Gregorio GB, Hensley L, Lu T, Ranganathan G, Kern PA. Lipid and carbohydrate metabolism in mice with a targeted mutation in the IL-6 gene: absence of development of age-related obesity. *Am J Physiol Endocrinol Metab*. 2004;287(1):E182–E187.
52. Fritsche L, et al. IL-6 deficiency in mice neither impairs induction of metabolic genes in the liver nor affects blood glucose levels during fasting and moderately intense exercise. *Diabetologia*. 2010;53(8):1732–1742.
53. Wallenius V, et al. Interleukin-6-deficient mice develop mature-onset obesity. *Nat Med*. 2002;8(1):75–79.
54. McKenzie GJ, Bancroft A, Grencis RK, McKenzie AN. A distinct role for interleukin-13 in Th2-cell-mediated immune responses. *Curr Biol*. 1998;8(6):339–342.
55. Reilly SM, et al. Nuclear receptor corepressor SMRT regulates mitochondrial oxidative metabolism and mediates aging-related metabolic deterioration. *Cell Metab*. 2010;12(6):643–653.
56. Liu S, et al. Role of peroxisome proliferator-activated receptor {delta}/{beta} in hepatic metabolic regulation. *J Biol Chem*. 2011;286(2):1237–1247.
57. Wang X, Yang Z, Xue B, Shi H. Activation of the cholinergic antiinflammatory pathway ameliorates obesity-induced inflammation and insulin resistance. *Endocrinology*. 2011;152(3):836–846.